Final Report for Project **1021**

Project title: **Paleo-Constraints on Monsoon Evolution and Dynamics (PACMEDY)**

Principal investigator: **Johann Jungclaus**

Report period: **Jan. 1, 2017 - Dec. 31, 2020**

1. Overview

The goal of the PACMEDY project was to provide and document a data base of paleoclimate simulations for the mid and late Holocene and to analyse the simulations assessing changes in the monsoon systems. PACMEDY partners AWI and MPI-M have carried out global simulations using comprehensive, state-of-the-art Earth System Models (ESM) with a focus on contributions to the PMIP4 initiative as part of CMIP6. Here PACMEDY groups contribute to the PMIP4 "midHolocene" time-slice experiment and to the transient simulations covering the last millennium (PMIP4 "past1000" and "past2k"). In addition, PACMEDY partners have provided new simulations covering the period from the mid Holocene (8 - 6kyr BP) to present.

2. Simulations carried out in PACMEDY

PACMEDY partners MPI-M and AWI have carried out simulations using MPI-ESM-1.2 (Mauritsen et al., 2019), the AWI-ESM (Sidorenko et al. 2019), and the isotope-enabled MPI-ESM-WISO (Cauquoin et al., 2019).

2.1 MidHolocene simulations as part of PMIP4

The time-slice experiment for the mid-Holocene (PMIP4 "midHolocene", Otto-Bliesner et al., 2017) have been conducted by **MPI-M and AWI**. The data sets have been uploaded to the CMIP6 ESGF data base (e.g. https://esgf-data.dkrz.de/search/cmip6-dkrz/). In addition to the standard "midHolocene" experiments, the groups have provided additional sensitivity experiments regarding the roles of dust and vegetation).

AWI has performed experiments under pre-industrial and different Holocene regimes with AWI-ESM, a state-of-the-art climate model with unstructured mesh and varying resolutions, to examine the sensitivity of the simulated Atlantic meridional overturning circulation (AMOC) to early-Holocene and mid Holocene insolation, GHGs, topography (including properties of the ice sheet), and glacial meltwater perturbation (Shi et al., 2020).

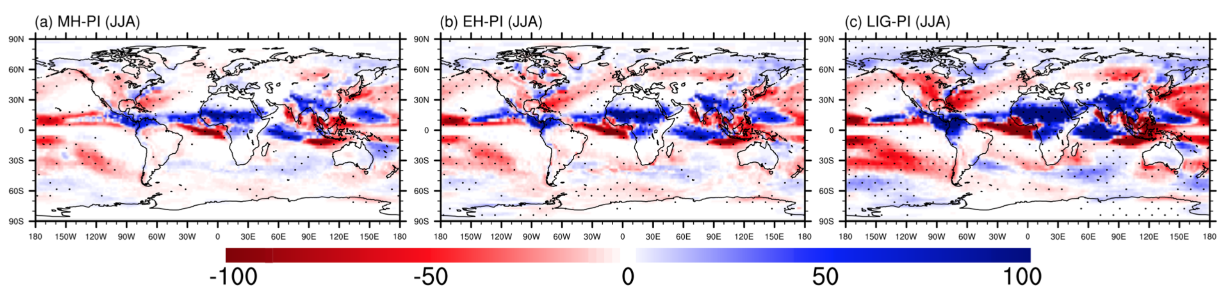

Figure 1. Summer precipitation anomalies in MH, EH and LIG relative to PI. Units: mm/month. The marked area has a significance level of above 95% based on Student's t-test.

Fig. 1 shows the JJA precipitation anomalies in three paleo scenarios, i.e., mid-Holocene (MH), early-Holocene (EH) and Last Interglacial (LIG), with respect to pre-industrial (PI) state based on AWI-ESM-1-1-LR. It is shown that in these warm episodes the rainfall increases over China, Indian, and Africa. Such pattern indicates a northward shift of Inter Tropical Convergence Zone (ITCZ) (Shi et al., 2020).

2.2 Transient simulations of Holocene climate

Simulations following the PMIP4 protocol for the last millennium (Jungclaus et al., 2017) have been conducted by PACMEDY partners CNRS-LSCE, MPI-MET, and Stockholm University. A unique feature of MPI-M's contribution is the extension in time to include the entire "Common Era", i.e. the last 2000 years (Jungclaus et al., 2017).

Going beyond the scope of PMIP4, PACMEDY has produced simulations covering the mid to late Holocene (8-6 kyrBP to present). These simulations feature many innovative aspects. While previous simulations have often used coarser-resolution versions for long-term simulations, the PACMEDY simulations are carried out with the same or similar model set-ups and complexity as the CMIP6 experiments for past, present, and future. In addition, new aspects have been considered, such as dedicated sensitivity experiments on vegetation, dust, or the role of external forcing.

AWI: Transient experiments for the past 6,000 years were performed using AWI-ESM2 with interactive vegetation feedbacks (Shi et al., 2020). We firstly conducted a 1,000-year spin-up run with the application of mid-Holocene boundary forcings, involving the orbital parameters and greenhouse gases (GHGs), according to the PMIP4 criterion [Otto-Bliesner et al., 2017]. The climate condition from the last model year in the spin-up run served as the initial state of the transient simulation. The transient orbital parameters are calculated according to Berger [1978]. The greenhouse gases are taken from the ice cores records in a recent study Kohler et al. [2017]. Moreover, as the change of topography from mid-Holocene to present is minor, we use constant topography under pre-industrial condition for the whole transient period. The atmosphere grid in the experiment is T63 (about 1.9 degree) with 47 vertical levels. A multi-resolution approach is employed in the ocean module. The ocean module applies up to 20 km horizontal resolution over the Arctic region and 150 km for the far field ocean. Moreover, the tropical belt has a refined resolution of 30-50 km. There are 46 uneven vertical depths in the ocean component.

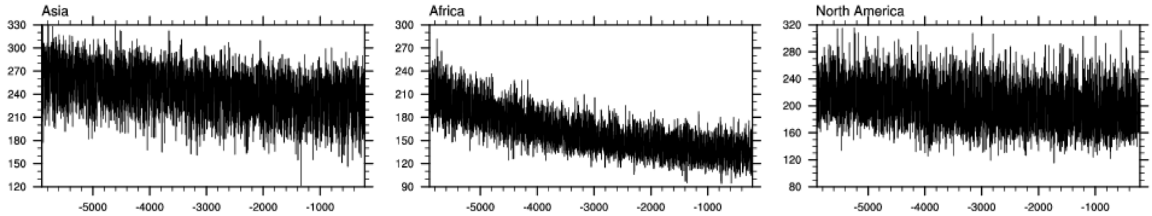

Figure 2. Evolution of monsoon precipitations for each monsoon domain. (mm/month)

Changes in the monsoon extent and strength are assessed using the following metrics: The monsoon extent is the land-only area where annual precipitation range, defined as the difference between summer and winter rainfall, exceeds 2 mm/day for each monsoon domain. The selected threshold warrants a concentrated summer rainy season and distinguishes monsoons from year-round rainy regimes. The monsoon strength is the average summer rainfall calculated in each monsoon domain:

1. Asian monsoon (5–23.3N, 60–120E).
2. African monsoon (5–23.3N, 15W-20E).
3. North American monsoon (0–30N, 120–40W).

The evolution of monsoon precipitation for each domain is shown in Fig. 2. The Asia and Africa monsoon experience a reduced monsoon rainfall from mid-Holocene to present, with the most pronounced trends being before 4k, after 4k the reducing speed is getting smaller. For North America, there is a general decrease from 6k to 4k, followed by no significant changes in monsoon rainfall.

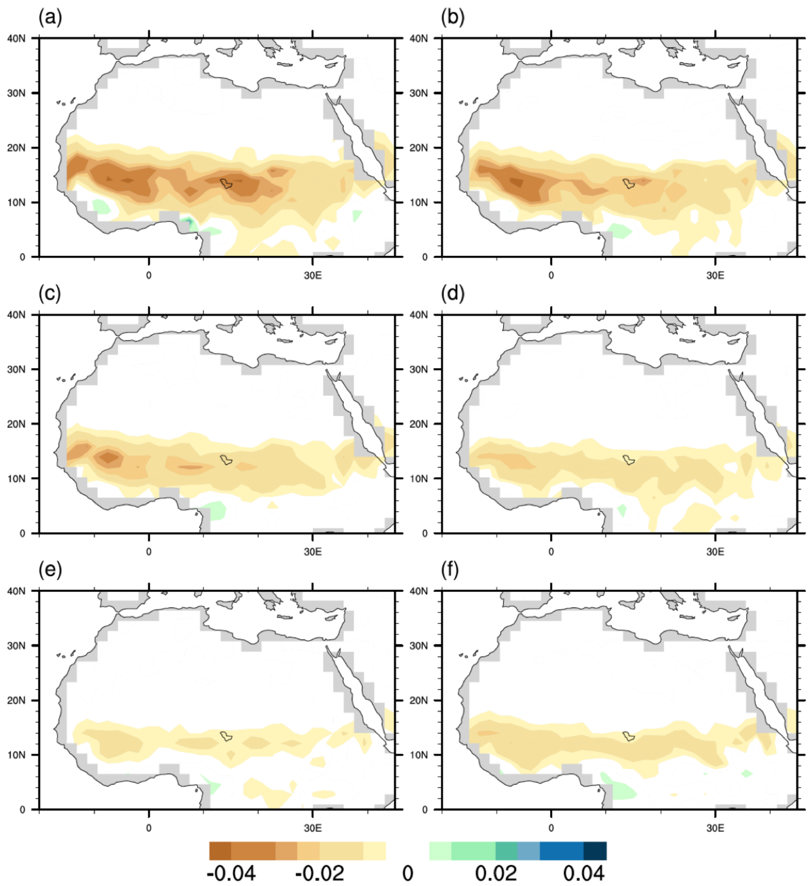

Figure 3. Trend of JJA precipitation for (a) 6k to 5k, (b) 5k to 4k, (c) 4k to 3k, (d) 3k to 2k, (e) 2k to 1k, and (f) 1k to 0k in Africa.

Fig.3 shows the trend of JJA precipitation over Africa for different periods in the past 6,000 years. The most intriguing feature is the dryness at 10-20^{o}N, which finds its greater expression from 6k to 4k. After 4k, such a trend is much less pronounced and limited in a narrower region (10-16^{o}N). The north extent of Africa summer monsoon rainfall experienced a southward displacement in the past 6,000 years, which reached up to 20^{o} N at 6k-5k, then stably maintained at 16-18 ^{o}N from 5k to 4k, followed by 14-16^{o}N for the rest time. In some special years during the past 2k, the north extent reached only 12^{o}N.

MPI-M: A suite of transient simulations from 8 kyr BP to 1850 CE was carried out with MPI-ESM 1.2 (Mauritsen et al., 2019). One experiment was performed using only orbital-induced insolation changes and variations in greenhouse gases. Another experiment applied in addition time-varying changes in solar irradiance and stratospheric sulfate aerosol injections from volcanoes, and, for the last millennium, land-use changes as in the PMIP4 past1000 experiment (Dallmeyer et al., 2020; Bader et al., 2020). While in the standard experiment CO_2 is prescribed, an additional experiment was carried out, where CO_2 is calculated interactively, but nudged to reconstructions by varying surface ocean alkalinity forcing (Brovkin et al. (2019).

We performed a spatio-temporal analysis of annual temperature variability during the Holocene using data from the MPI-ESM simulations with fast-varying solar (TSI, SSI) and volcanic forcing (Bader et al., 2020). The global spatial patterns of the warming and cooling modes exhibit different centers of action (Fig. 4). The warming mode is mainly related to the combined effect of increasing greenhouse gases and the latitude-dependent trend in annual mean insolation. The warming mode is most pronounced in the tropics. The simulated cooling mode – resembling the global cooling trend shown by some reconstructions – is determined by changes in the seasonal cycle of Arctic sea-ice that are forced by orbital variations and volcanic eruptions. This mode predominantly affects the Arctic, North Atlantic and Eurasian regions. The warming mode dominates in the mid-Holocene, whereas the cooling mode takes over in the late Holocene. Moreover, the weighted sum of the two modes yields the simulated global temperature trend evolution during the Holocene.

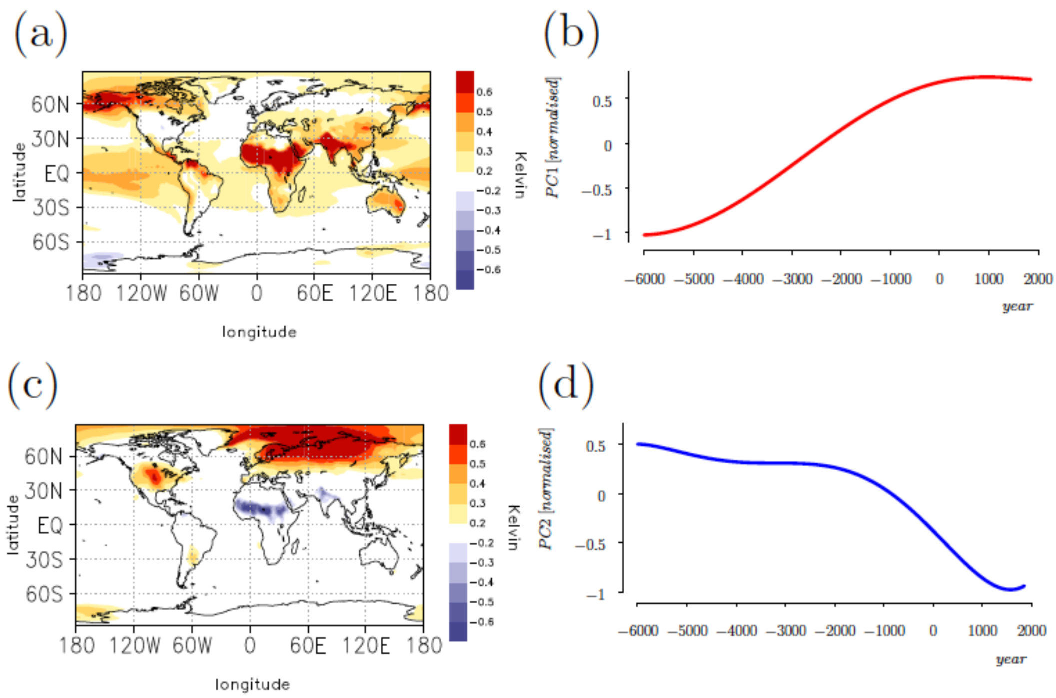

Fig. 4: The simulated warming and cooling mode in the transient Holocene simulation. First two spatial EOF modes (a, c) and corresponding normalised smoothed PCs (b,d) based on the simulated annual 2 meter temperature using the MPI-ESM data. The red and blue curve in the right panels show the low-pass filtered PCs. The explained variances of the annual (not low-pass filtered) temperature modes are: 18% and 9% (from Bader et al., 2020).

Experiments with different external forcing factors show a substantial effect of higher frequency variability of the external forcing – like volcanoes – on the trend development of the global mean temperature. Integration these effects (predominantly by the oceans) affects also the centennial to millennial variations (Fig. 5). The slope of the spectra calculated between periods of 2 to 400 years show a considerable increase with much higher power on centennial time scales. This highlights the importance of accounting for high-frequency external forcing factors.

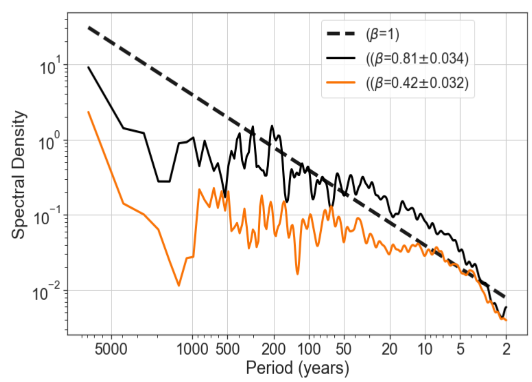

Fig. 5: Variability characteristics of the global mean surface temperature (GMST) in two MPI-ESM transient Holocene simulations: Power spectra of GMST for (black) the experiment with all forcings (including volcanoes), and (orange) the simulations driven only by the slowly-varying orbital and greenhouse-gas forcings. The dashed black line indicates a slope of one that indicates long-term memory behaviour (Jungclaus et al., manuscript in preparation).

3. Results: Factors controlling ITCZ and monsoon precipitation

One goal of PaCMEDy was to isolate the factors controlling ITCZ and monsoon precipitation and determine whether they influence future climate projections. We have analysed how the ITCZ and monsoonal precipitation intensity change in past (*mid-Holocene*) and future (*rcp8.5*) climate model simulations relative to the pre-Industrial times (*piControl*) from PMIP3 - CMIP5 archives, focusing only on summer seasons (JJAS for the Northern and DJFM for the Southern Hemisphere). We have used the multimodel ensemble of 9 models which have the three experiments (bcc-csm-1-1, CCSM4, CNRM-CM5, CSIRO-Mk3-6-0, FGOALS-g2, HadGEM2-ES, IPSL-CM5A-LR, MIROC-ESM and MRI-CGCM) to isolate robust responses to external forcing, while intermodel differences were useful to understand structural uncertainties on monsoon behaviors (D'Agostino et al., 2019, 2020).

3.1 Monsoon response to orbital forcing versus green-house gases (Northern Hemisphere)

In the Northern Hemisphere, the future *rcp8.5* global warming signal is much stronger than the *mid-Holocene* past relative to *piControl* (+4.2 K and +0.3 K, respectively), the two experiments show larger interhemispheric thermal contrasts than *piControl* (+10.0 K and +9.7 K compared to +9.2 K for *piControl*). However, the precipitation difference between *rcp8.5* and *mid-Holocene* (Fig. 6c) reveals a complex pattern of relative drying and wettening, reflective of a general tendency towards land drying and ocean wettening in *rcp8.5*, and land wettening and ocean drying in *mid-Holocene*.

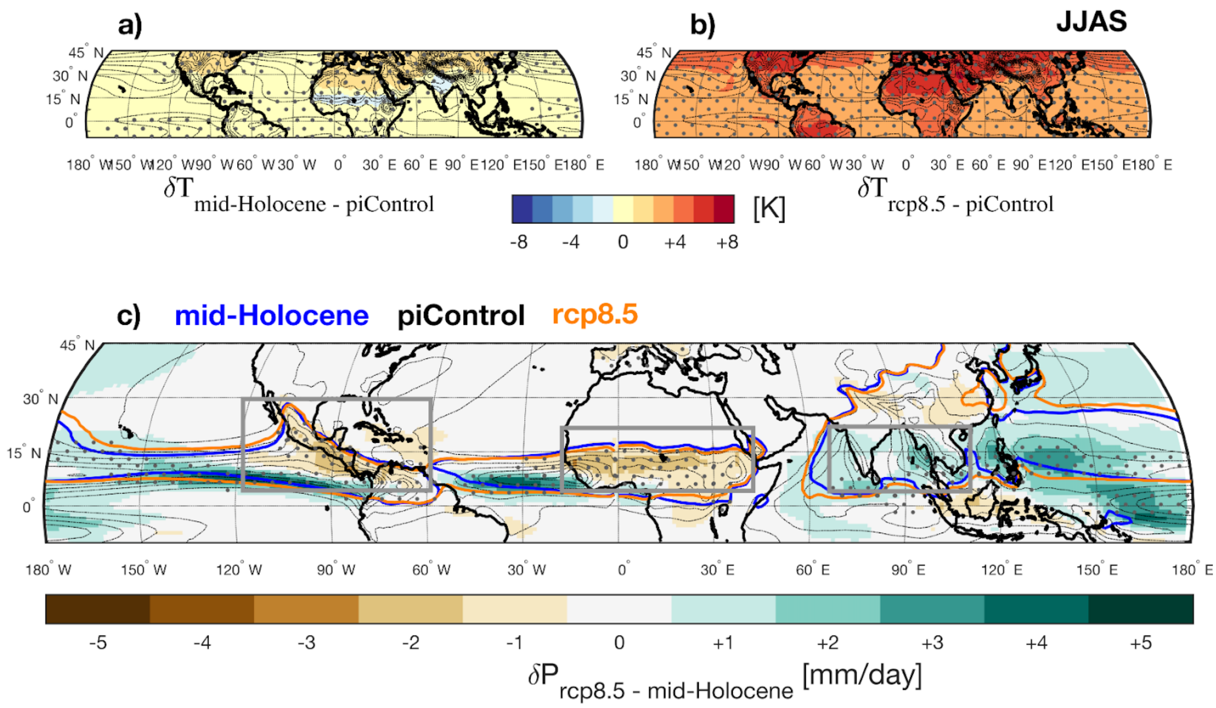

Fig. 6: Surface temperature difference between *mid-Holocene* (a) and *rcp8.5* (b) and *piControl* in June-to-September (JJAS) ensemble means (shading). Precipitation difference between *rcp8.5* and *mid-Holocene* JJAS ensemble means (c, shading). Black dashed lines in every panel show the *piControl* as reference (contour interval 2 K for temperature and 2 mm/day for precipitation). Orange and blue bold lines in c) show areas within which the annual precipitation range (JJAS minus DJFM) exceeds 2 mm/day for *rcp8.5* and *mid-Holocene*, respectively. Grey boxes indicate the North American, African and Indian monsoon domains. Stippling indicates areas where at least 8 out of 9 models agree on the sign of the change.

3.2 Monsoon response to orbital forcing versus green-house gases (Southern Hemisphere)

In the Southern Hemisphere, we have found contrasting results on monsoon response between the future *rcp8.5* and the *mid-Holocene* past relative to *piControl*. Southern Hemisphere monsoons were weaker than pre-Industrial times while they are stronger in the *rcp8.5.* However, the precipitation difference between *rcp8.5* and *mid-Holocene* (Fig. 7c) reveals a complex pattern of relative drying and wettening, reflective of a general tendency towards land drying and ocean wettening in *rcp8.5*, and land wettening and ocean drying in *mid-Holocene*.

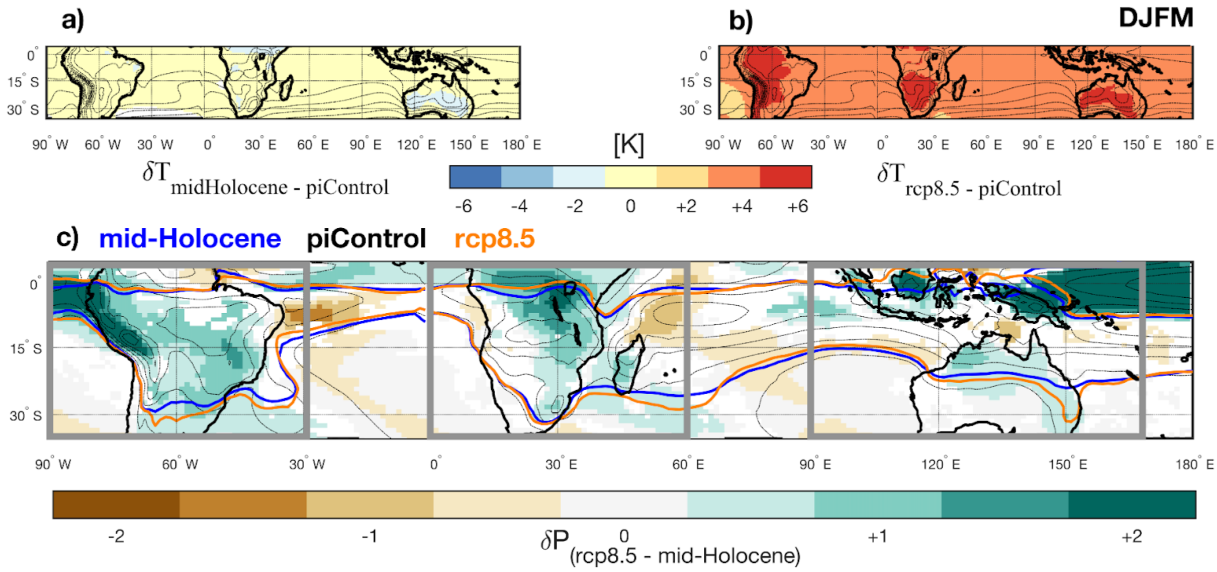

Fig. 7: Surface temperature difference between *mid-Holocene* (a) and *rcp8.5* (b) and *piControl* in December-to-March (DJFM) ensemble means (shading). Precipitation difference between *rcp8.5* and *mid-Holocene* DJFM ensemble means (c, shading). Black dashed lines in every panel show the *piControl* as reference (contour interval 2 K for temperature and 2 mm/day for precipitation). Orange and blue bold lines in c) show areas within which the annual precipitation range (DJFM minus JJAS) exceeds 2 mm/day for *rcp8.5* and *mid-Holocene*, respectively. Grey boxes indicate the South American, South African and Australian monsoon domains. Only values where at least 8 out of 9 models agree on the sign of the change are shown.

3.3 The energetic framework

Important steps forward to better understand the complex response of monsoons to cl imate change have been made by linking the tropical rainfall and atmospheric circulation response to the net energy input (NEI) change (Biasutti et al. 2018; D'Agostino et al. 2019). Analysis of the energy budget applied to the global mean precipitation may provide further insights into what controls regional rainfall changes (Levermann et al. 2009; Muller and O'Gorman 2011; O'Gorman et al. 2012). Within this framework, monsoons are viewed as moist energetically direct circulations tightly connected to the Hadley Circulation (Bordoni and Schneider 2008; Schneider et al. 2014; Biasutti et al. 2018). As fundamental components of the tropical overturning circulation, monsoons act to export moist static energy (MSE) away from their ascending branches and precipitation maxima. If vertically integrated eddy MSE flux due to the mean flow is negligible, the NEI flux into the atmospheric column, given by the difference between top-of-atmosphere radiative and surface energy fluxes, is primarily balanced by divergence of vertically integrated MSE flux in a steady state, which is describing P-E change in the tropics (Neelin and Held 1987; Chou et al. 2001; Merlis et al. 2013; Boos and Korty 2016). In particular, Muller and O'Gorman (2011) argue that changes in radiative and surface sensible heat fluxes provide a guide to the local precipitation response over land. Therefore, any changes in NEI (for example related to precession-induced insolation changes, aerosols, greenhouse gases induced by global warming and others) require anomalous meridional energy transport to restore the energy balance. Given that, during the summer, most of this transport is carried out by monsoonal circulations (Heaviside and Czaja 2013; Walker 2017), this would imply a shift of the monsoonal circulation ascending branches and precipitation maxima into the hemisphere with increased NEI and, possibly, an associated meridional atmospheric circulation strengthening (Schneider et al. 2014; Bischoff et al. 2017). The degree to which changes in energy transport implied by a given radiative forcing are accomplished through just changes in circulation strength (dynamical factors) or changes in energy stratification (thermodynamical factors) is still debated. In order to attribute monsoonal changes to either moisture content changes or atmospheric circulation changes, we have decomposed the moisture budget in thermodynamic and dynamic contributions (Trenberth and Guillemot,1995; Seager et al., 2010).

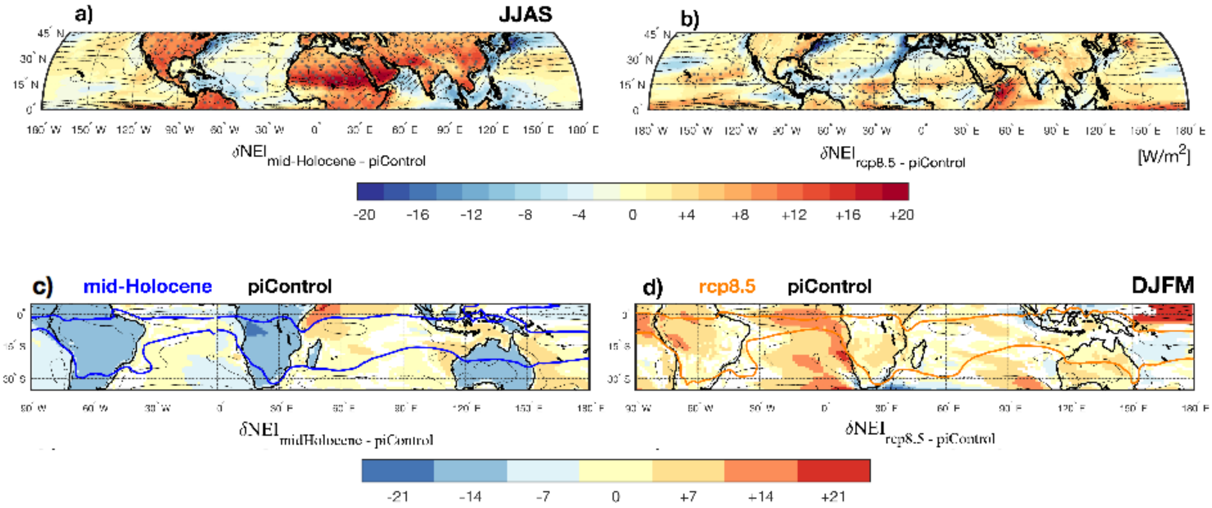

Fig. 8: Net energy input (NEI) difference between mid-Holocene (a, c) and rcp8.5 (b, d) relative to piControl in June-to-September (JJAS, upper panels) and in December-to-March (DJFM, lower panels) ensemble means (shading). Black dashed lines in each panel show the piControl as reference (contour interval 20 W/m). Stippling in upper panels indicates areas where at least 8 out of 9 models agree on the sign of the change. In lower panels only areas where at least 8 out of 9 models agree on the sign of the change are shown.

Figure 8 shows that *rcp8.5* and *mid-Holocene* have very different NEI structure and this would likely explain the different monsoon response in the two experiments: i.e. monsoons are weaker where the anomalous NEI is negative relative to *piControl* and vice-versa. In JJAS (Fig. 8a), *mid-Holocene* NEI is positive all over Northern Hemisphere land, hence the atmospheric circulations needs to be stronger in order to export away energy from the ascending branches of the monsoonal circulation, with associated increased precipitation. The opposite is for *mid-Holocene* DJFM (Fig. 8c), when Southern Hemisphere monsoons were weaker than pre-Industrial conditions. Therefore, monsoons changes in the *mid*-Holocene are dominated by dynamical factors (Fig. 9). On the other hand, for both JJAS and DJFM (Fig. 8b and d), the anomalous NEI is quite homogeneous without a strict land/ocean contrast, as in the *mid-Holocene*. This means that monsoonal response is very regional and depends on the thermodynamics and vertical stratification of the atmosphere.

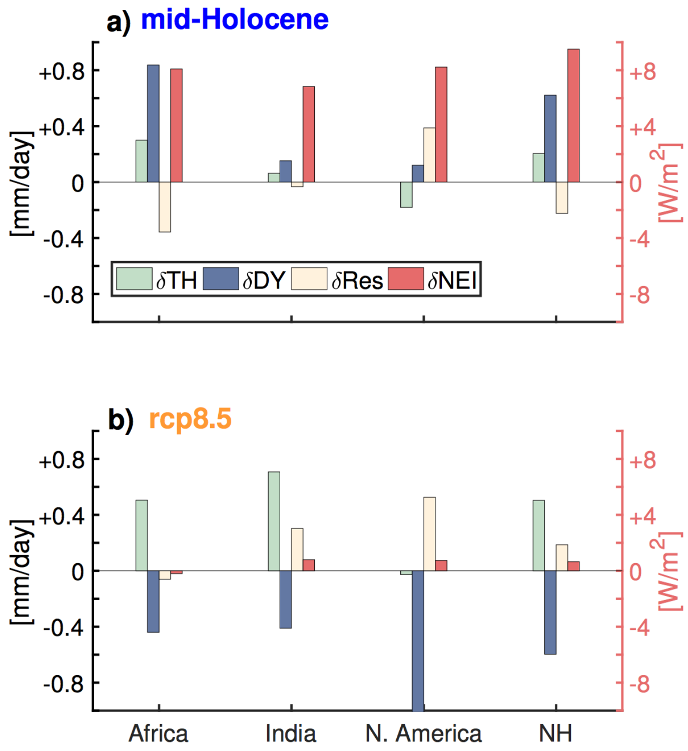

Fig. 9: Regionally averaged Net Energy Input (NEI - red axis) changes and changes in thermodynamic (δTH) and dynamic (δDY) components of the moisture budget, as well as its residual (δRes) for mid-Holocene (a) and rcp8.5 (b) (black axis) for Northern Hemisphere monsoons. Note that 8 out of 9 models agree on the sign of the change.

References (in bold for publications from PACMEDY)

Bader, J.; Jungclaus, J.; Krivova, N.; Lorenz, S.; and Claussen, M., 2020: Global temperature modes shed light on the Holocene temperature conundrum", *Nature Communications*, *11*: 4726. doi:10.1038/s41467-020-18478-6 .

Biasutti, M., and Coauthors, 2018: Global energetics and local physics as drivers of past, present and future monsoons. Nature Geoscience, 11 (6), 392.

Bischoff, T., T. Schneider, and A. N. Meckler, 2017: A conceptual model for the response of tropical rainfall to orbital variations. Journal of Climate, 30 (20), 8375–8391.

Boos, W. R., and R. L. Korty, 2016: Regional energy budget control of the intertropical convergence zone and application to mid-Holocene rainfall. Nature Geoscience, 9 (12), 892.

Bordoni, S., and T. Schneider, 2008: Monsoons as eddy-mediated regime transitions of the tropical overturning circulation. Nature Geoscience, 1(8), 515.

Brierley, C. and Wainer, I., 2018. Inter-annual variability in the tropical Atlantic from the Last Glacial Maximum into future climate projections simulated by CMIP5/PMIP3. Climate of the Past, 14(10), pp.1377-1390.

Brovkin, V., Lorenz, S., Raddatz, T., Ilyina, T., Stemmler, I., Toohey, M., and Claussen, M.: What was the source of the atmospheric CO2 increase during the Holocene?, Biogeosciences, 16, 2543–2555, https://doi.org/10.5194/bg-16-2543-2019, 2019.

Chou, C., J. Neelin, and H. Su, 2001: Ocean-atmosphere-land feedbacks in an idealized monsoon. Quarterly Journal of the Royal Meteorological Society, 127 (576), 1869–1891.

Cauquoin, A., Werner, M., and Lohmann, G., 2019: Water isotopes – climate relationships for the mid-Holocene and preindustrial period simulated with an isotope-enabled version of MPI-ESM. Clim. Past, 15, 1913–1937. doi:10.5194/cp-15-1913-2019

Cauquoin, A; Werner, M; Lohmann, G (2020): MPI-ESM-wiso simulations data for preindustrial and mid-Holocene conditions. PANGAEA, doi:10.1594/PANGAEA.912258

Dallmeyer, A. Claussen, M., Lorenz, S.J., Shanahan, T.: The end of the African humid period as seen by a transient comprehensive Earth system model simulation of the last 8000 years, Clim. Past, 16, 117–140, doi: 10.5194/cp-16-117-2020, 2020.

D'Agostino, R., Bader, J., Bordoni, S., Ferreira, D. & Jungclaus, J., 2019: Northern hemisphere monsoon response to mid-holocene orbital forcing and greenhouse gas-induced global warming. *Geophysical Research Letters*, *46*, 1591-1601. doi:10.1029/2018GL081589.

D'Agostino, R., Brown, J., Moise, A., Nguyen, H., Silva Dias, P. & Jungclaus, J.H., 2020: Contrasting southern hemisphere monsoon response: mid-Holocene orbital forcing versus future greenhouse-gas induced global warming. *Journal of Climate*, *33*, 9595-9613. doi:10.1175/JCLI-D-19-0672.1.

Heaviside, C., and A. Czaja, 2013: Deconstructing the Hadley Cell heat transport. Quarterly Journal of the Royal Meteorological Society, 139 (677), 2181–2189.

Jungclaus, J. H., et al.: The PMIP4 contribution to CMIP6 – Part 3: The last millennium, scientific objective, and experimental design for the PMIP4 past1000 simulations, Geosci. Model Dev., 10, 4005–4033, https://doi.org/10.5194/gmd-10-4005-2017, 2017.

Levermann, A., J. Schewe, V. Petoukhov, and H. Held, 2009: Basic mechanism for abrupt monsoon transitions. Proceedings of the National Academy of Sciences, 106 (49), 20 572–20 577.

Mauritsen, T., et al.: Developments in the MPI-M Earth System Model version 1.2 (MPI-ESM 1.2) and its response to increasing CO2. Journal of Advances in Modeling Earth Systems, 11, 998-1038, doi: 10.1029/2018MS001400, 2019.

Merlis, T., T. Schneider, S. Bordoni, and I. Eisenman, 2013: Hadley circulation response to orbital precession. Part I: Aquaplanets. Journal of Climate, 26 (3), 740–753.

Muller, C., and P. O'Gorman, 2011: An energetic perspective on the regional response of precipitation to climate change. Nature Climate Change, 1 (5), 266.

Neelin, J., and I. Held, 1987: Modelling tropical convergence based on the moist static energy budget. Monthly Weather Review, 115 (1), 3–12.

O'Gorman, P. A., R. P. Allan, M. P. Byrne, and M. Previdi, 2012: Energetic constraints on precipitation under climate change. Surveys in geophysics, 33 (3-4), 585–608.

Otto-Bliesner, B.L., et al.: The PMIP4 contribution to CMIP6 – Part 2: Two interglacials, scientific objective and experimental design for Holocene and Last Interglacial simulations, Geosci. Model Dev., 10, 3979–4003, https://doi.org/10.5194/gmd-10-3979-2017, 2017.

Seager, R., N. Naik, and G. A. Vecchi, 2010: Thermodynamic and dynamic mechanisms for large-scale changes in the hydrological cycle in response to global warming. Journal of Climate, 23 (17), 4651–4668.

Schneider, T., T. Bischoff, and G. H. Haug, 2014: Migrations and dynamics of the intertropical convergence zone. Nature, 513 (7516), 45–53.

Sidorenko et al. 2019: Evaluation of FESOM2.0 coupled to ECHAM6.3: Pre-industrial and HighResMIP simulations. Journal of Advances in Modeling Earth Systems, 11, DOI: 10.1029/2019MS001696

Shi, X., Lohmann, G., Sidorenko, D., Yang, H. 2020 : Early-Holocene simulations using different forcings and resolutions in AWI-ESM. The Holocene. 10.1177/0959683620908634

Shi, X., and G. Lohmann, 2019: The Northern Hemisphere synoptic processes under early-Holocene regimes. Journal of Geophysical Research - Atmospheres (submitted)

Trenberth, K. E., and C. J. Guillemot, 1995: Evaluation of the global atmospheric moisture budget as seen from analyses. Journal of Climate, 8 (9), 2255–2272.